A Generic and Multi-Functional Electromagnetic Transient Model for Grid-Following Inverter

Preprint

Soham Chakraborty,[1] Jing Wang,[1] Rasel Mahmud,[1] Andy Hoke,[1] Brian Johnson,[2] Romulo Goncalves Bainy,[2] and Hangtian Lei[2]

1 National Renewable Energy Laboratory
2 University of Idaho

Presented at the 52nd IEEE Photovoltaic Specialists Conference
Seattle, Washington
June 9–14, 2024

NREL is a national laboratory of the U.S. Department of Energy
Office of Energy Efficiency & Renewable Energy
Operated by the Alliance for Sustainable Energy, LLC

This report is available at no cost from the National Renewable Energy Laboratory (NREL) at www.nrel.gov/publications.

Contract No. DE-AC36-08GO28308

Conference Paper
NREL/CP-5D00-88660
November 2024

A Generic and Multi-Functional Electromagnetic Transient Model for Grid-Following Inverter

Preprint

Soham Chakraborty,[1] Jing Wang,[1] Rasel Mahmud,[1] Andy Hoke,[1] Brian Johnson,[2] Romulo Goncalves Bainy,[2] and Hangtian Lei[2]

1 National Renewable Energy Laboratory
2 University of Idaho

Suggested Citation
Chakraborty, Soham, Jing Wang, Rasel Mahmud, Andy Hoke, Brian Johnson, Romulo Goncalves Bainy, and Hangtian Lei. 2024. *A Generic and Multi-Functional Electromagnetic Transient Model for Grid-Following Inverter: Preprint*. Golden, CO: National Renewable Energy Laboratory. NREL/CP-5D00-88660. https://www.nrel.gov/docs/fy25osti/88660.pdf.

NREL is a national laboratory of the U.S. Department of Energy
Office of Energy Efficiency & Renewable Energy
Operated by the Alliance for Sustainable Energy, LLC

This report is available at no cost from the National Renewable Energy Laboratory (NREL) at www.nrel.gov/publications.

Contract No. DE-AC36-08GO28308

Conference Paper
NREL/CP-5D00-88660
November 2024

National Renewable Energy Laboratory
15013 Denver West Parkway
Golden, CO 80401
303-275-3000 • www.nrel.gov

NOTICE

This work was authored in part by the National Renewable Energy Laboratory, operated by Alliance for Sustainable Energy, LLC, for the U.S. Department of Energy (DOE) under Contract No. DE-AC36-08GO28308. Funding provided by U.S. Department of Energy Office of Energy Efficiency and Renewable Energy Solar Energy Technologies Office. The views expressed herein do not necessarily represent the views of the DOE or the U.S. Government. The U.S. Government retains and the publisher, by accepting the article for publication, acknowledges that the U.S. Government retains a nonexclusive, paid-up, irrevocable, worldwide license to publish or reproduce the published form of this work, or allow others to do so, for U.S. Government purposes.

Cover Photos by Dennis Schroeder: (clockwise, left to right) NREL 51934, NREL 45897, NREL 42160, NREL 45891, NREL 48097, NREL 46526.

A Generic and Multifunctional Electromagnetic Transient Model for Grid-Following Inverters

Soham Chakraborty[1], Jing Wang[1], Rasel Mahmud[1], Andy Hoke[1],
Brian Johnson[2], Romulo Goncalves Bainy[2], and Hangtian Lei[2]
[1] Power Systems Engineering Center, National Renewable Energy Laboratory, Golden, Colorado 80401, USA,
[2] Electrical and Computer Engineering, University of Idaho, Moscow, Idaho, 83844, USA.
{soham.chakraborty, jing.wang, rasel.mahmud, andy.hoke}@nrel.gov, {bjohnson, romulo, hlei7}@uidaho.edu

***Abstract*—This paper presents a generic and multifunctional electromagnetic transient (EMT) dynamic model of grid-following (GFL) inverter-based resources (IBRs) using the PSCAD software platform. The features of the model include flexibility in selecting various types and combinations of DC sources covering photovoltaic modules, battery modules, and ideal DC-source modules as well as flexibility in selecting either switching or averaged models of the inverter. This model also covers exhaustive lists of controller algorithm, including open-loop/closed-loop PQ dispatch control, DC voltage and AC terminal voltage control, and conventional current control designed in the dq-domain, the $\alpha\beta$-domain, and the positive-/negative-sequence domain. Moreover, this model is equipped with flexibility in selecting various types of current-limiting schemes, including saturation-based and latching-based current limiters, and anti-windup protection. Also, the EMT model is agnostic to the MVA rating and is suitable for interfacing transmission systems by complying with IEEE Std. 2800. The generality in the power circuits and the multifunctional options in the operation and control of the developed EMT model make it suitable for both academia and industry to study various power system aspects, including, but not limited to, the fault behavior of GFL IBRs, the impacts on the protection system, and the transient stability of a system interfaced with large numbers of GFL IBRs.**

I. Introduction

Inverter-based resources (IBRs) are replacing traditional fossil fuel-based synchronous generators at a remarkable pace, driven by the urgent pursuit of net-zero energy emissions and the ambitious target of achieving 100% renewable energy by 2050. IBRs possess dynamics that significantly differ from those of synchronous generator-based sources, especially as IBR penetrations increase and the differences are more obvious [1]. The system dynamics need to be revisited to fundamentally understand IBR dynamics, how IBRs affect the overall system stability, and other major considerations, e.g., the protection system [2], [3]. Fig. 1 shows a power system timescale. The timescale of the IBR control is between multiple microseconds and multiple miniseconds, and it is much smaller than that of the synchronous generator. The wave and electromagnetic phenomena are of particular interest for an IBR-dominant system. Overall, modeling IBRs provides a fundamental understanding of IBR-related dynamics; therefore, developing high-fidelity IBR models has been an urgent and mandatory task for academia and industry. Among the efforts, developing an electromagnetic transient (EMT) model is a high priority because the EMT model provides the necessary and accurate transients for stability analysis and fault studies, as shown in Fig. 1. Modeling the aspects of IBRs is an individual effort, done case by case, depending on the purpose of the study. A few examples are described here.

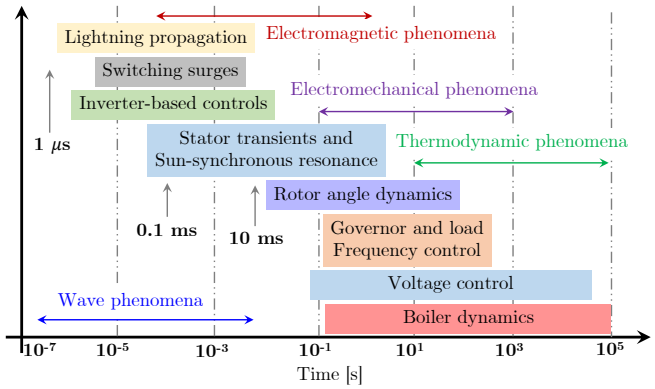

Fig. 1. Power system timescale [4].

A real-world microgrid with 100% renewable is simulated in PSCAD to study the transient dynamics of a microgrid with "detailed" models of grid-forming (GFM) and grid-following (GFL) inverters [5]. The EMT model, however, is limited to outer PQ dispatch control, with the inner current controller designed in the dq domain while complying with IEEE Std. 1547-2018 [6]. Open-source PSCAD GFL and GFM inverters interfaced with a 9-bus network are developed in [7] to benchmark the IBR modeling for a transient study. This EMT model develops the conventional dq domain current and voltage controller for GFL and GFM IBRs, respectively, with various functionalities, such as synthetic inertia and voltage control-based grid support for GFL IBRs and automatic generation control and virtual resistance control for the GFM IBRs. An EMT numerical simulation algorithm, applied to the high-fidelity switching system model of a photovoltaic (PV) plant, is implemented in [8] using PSCAD with Fortran and the C/C++ environment for high-performance computations

This work was authored in part by the National Renewable Energy Laboratory, operated by Alliance for Sustainable Energy, LLC, for the U.S. Department of Energy (DOE) under Contract No. DE-AC36-08GO28308. Funding provided by U.S. Department of Energy Office of Energy Efficiency and Renewable Energy Solar Energy Technologies Office. The views expressed in the article do not necessarily represent the views of the DOE or the U.S. Government. The U.S. Government retains and the publisher, by accepting the article for publication, acknowledges that the U.S. Government retains a nonexclusive, paid-up, irrevocable, worldwide license to publish or reproduce the published form of this work, or allow others to do so, for U.S. Government purposes.

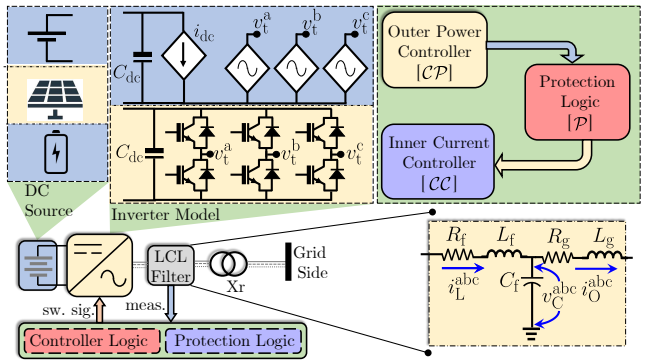

Fig. 2. Fundamental building blocks of the EMT model of GFL IBRs.

TABLE I
Parameters of the EMT model of GFL IBRs.

Inverter	Value of the Parameters
Ratings (3-ϕ)	480 V (L-L), 60 Hz, 1.25 MVA
DC side	$V_{\rm dc}$ = 1200 V, $f_{\rm sw}$ = 5 kHz
LCL silter	$L_{\rm f}$ = 15 μH, $L_{\rm g}$ = 1.5 μH, $C_{\rm f}$ = 280 μF

TABLE II
Available options in the developed EMT model of GFL IBRs for selecting the "DC source" type and "inverter model."

DC Source [$\mathcal{S}$]	Inverter Model [$\mathcal{M}$]
$\mathcal{S}1$: PV module $\mathcal{S}2$: Battery module	$\mathcal{M}1$: switching model
$\mathcal{S}3$: Ideal voltage source $\mathcal{S}4$: Any combination	$\mathcal{M}2$: Averaged model

and optimizations. A PV GFL IBR model is developed in [9] using PSCAD that is suitable for transmission-connected plants that comply with IEEE Std. 2800 [10]. Overall, the existing state of the art usually covers some aspects of IBR modeling, including the type of DC source, type of inverter model, inverter power-level control, inverter device-level control (current and/voltage control), measurements and grid synchronization, grid requirements control, and current limiting [11], but these models are not comprehensive enough to showcase multiple aspects, including balanced/unbalanced fault behavior, system dynamics, and stability etc. Therefore, this article goes beyond the state of the art and aims to develop a comprehensive GFL inverter model for transient stability studies, fault studies, and protection design. The contributions of this article are as follows. The EMT model developed in this work using the PSCAD platform:

1) Can be used as a single black box with flexibility in selecting the MVA rating.
2) Is suitable for interfacing transmission systems and complies with IEEE Std. 2800 [10]; therefore, the model could be of use to transmission system planners to study site-specific performance with IBR integration.
3) Is suitable for interfacing various types and combinations of DC sources, including the PV module, battery module, and ideal voltage source; therefore, this model could be of use to different vendors of GFL IBRs with varieties of DC sources.
4) Covers both switching models and averaged models. This provides a benchmark platform to study the impact of inverter modeling on various aspects, such as fault behavior.
5) Includes large sets of control logic, where the user can make a selection by choosing the correct flags, as described in Section II. The control logic covers an exhaustive list of active power control, reactive power control, and inner current control, as tabulated in Table III. The control architecture of commercial GFL IBRs is usually proprietary and can vary from one manufacturer to another. This generic EMT model can be used by both academia and industry to study the operation of systems with multivendor GFL IBRs.
6) Includes large sets of protection logic, where the user can make a selection by choosing the correct flags, as described in Section II. The protection logic covers an exhaustive list of the instantaneous current saturation limiter, instantaneous circular current limiter, current latching limiter, and anti-windup protections, as tabulated in Table III. It is well studied that the choice of limiter protection immensely impacts the fault behavior of IBRs; therefore, this model will be of use for protection system engineers to study and design suitable protection systems with GFL IBRs interfaced in the system.

II. Birds-Eye View of the EMT Model of GFL IBRs

The fundamental building blocks of the EMT model of GFL IBRs are shown in Fig. 2. The power circuit consists of the "inverter model" interfaced with the "DC source" of voltage, $V_{\rm dc}$. At the output terminals, an LCL filter ($L_{\rm f}$, $C_{\rm f}$, $L_{\rm g}$, and associated equivalent series resistances, $R_{\rm f}$ and $R_{\rm g}$, of the inductors) are connected and interfaced to the grid/network via a transformer. The main controller is responsible for generating the pulse-width modulated switching signals for the inverter based on processing the measurements (inner inductor current measurements, $i_{\rm L}^{\rm abc}$, output current measurements, $i_{\rm O}^{\rm abc}$, and capacitor voltage measurements, $v_{\rm C}^{\rm abc}$) via the "controller logic" and "protection logic." The rating and the parameters of the GFL IBR are tabulated in Table I. Note that the MVA rating is user-defined and can be changed based on the end-user requirement. The EMT model is connected to a 34.5-kV grid via a step-up transformer of the rating of the three-phase, 0.48/34.5-kV, 1.5-MVA Y-Δ transformer; however, this external circuit is independent of the model of GFL IBRs. The main features of the EMT model of GFL IBRs are as follows:

1) From the "DC source" model side, the developed EMT model has the flexibility to select various types of DC sources (single or combination) by choosing the flag, $\mathcal{S}$, externally, as tabulated in Table II. For example, $\mathcal{S} = \mathcal{S}1$ enables connecting a single PV module on the DC side, $\mathcal{S} = \mathcal{S}2$ enables connecting a single battery module on the DC side, $\mathcal{S} = \mathcal{S}3$ enables connecting a single ideal DC module on the DC side, and $\mathcal{S} = \mathcal{S}4$ enables connecting any combination of PV, battery, and ideal DC module on the DC side.
2) From the "inverter model" side, the developed EMT model has the flexibility to select two types of models by choosing the flag, $\mathcal{M}$, externally, as tabulated in Table II. For example, $\mathcal{M} = \mathcal{M}1$ enables the switching model, and $\mathcal{M} = \mathcal{M}2$ enables the averaged model of the inverter [12], [13].
3) From the "controller logic" side, the developed EMT model has the flexibility to select various types of controls, as tabulated in Table III. For example, in the "outer power" controller

TABLE III
Available options in the developed EMT model of GFL IBRs for selecting the "controller logic." and "protection logic."

Controller Logic [$\mathcal{C}$]		
Outer Power [$\mathcal{CP}$]		**Inner Current** [$\mathcal{CC}$]
Active Power [$\mathcal{CPP}$]	**Reactive Power** [$\mathcal{CPQ}$]	$\mathcal{CC}1$: dq domain
$\mathcal{CPP}1$: Open-loop P dispatch	$\mathcal{CPQ}1$: Open-loop Q dispatch	$\mathcal{CC}2$: $\alpha\beta$ domain
$\mathcal{CPP}2$: Closed-loop P dispatch	$\mathcal{CPQ}2$: Closed-loop Q dispatch	$\mathcal{CC}3$: Sequence domain
$\mathcal{CPP}3$: $V_{\rm dc}$ control	$\mathcal{CPQ}3$: $V_{\rm ac}$ control	

Protection Logic [$\mathcal{P}$]		
Current Limiter [$\mathcal{PC}$]		**Windup** [$\mathcal{PW}$]
Saturation – based [$\mathcal{PCS}$]		$\mathcal{PW}1$: Anti-windup for PI controller.
$\mathcal{PCS}1$: d-axis priority	$\mathcal{PCS}2$: q-axis priority	
Latching – based [$\mathcal{PCL}$]		$\mathcal{PW}2$: Anti-windup for PR controller.
$\mathcal{PCL}1$: d-axis priority	$\mathcal{PCL}2$: q-axis priority	

($\mathcal{CP}$), for active power control, open-loop P dispatch ($\mathcal{CPP} = \mathcal{CPP}1$), closed-loop P dispatch ($\mathcal{CPP} = \mathcal{CPP}2$), and DC-bus voltage control ($\mathcal{CPP} = \mathcal{CPP}3$) are available. Similarly, for reactive power control, open-loop ($\mathcal{CPQ} = \mathcal{CPQ}1$) Q dispatch, closed-loop ($\mathcal{CPQ} = \mathcal{CPQ}2$) Q dispatch, and AC terminal voltage control ($\mathcal{CPQ} = \mathcal{CPQ}3$) are available. In the "inner current" controller ($\mathcal{CC}$), the controller in the dq domain ($\mathcal{CC} = \mathcal{CC}1$), the controller in the $\alpha\beta$ domain ($\mathcal{CC} = \mathcal{CC}2$), and the controller in the sequence domain ($\mathcal{CC} = \mathcal{CC}3$) are available. The mathematical models of all these control logics are discussed in Section III.

4)] From the "protection logic" side, the developed EMT model has the flexibility to select various types of protections, as tabulated in Table III. For example, in the "current limiter" ($\mathcal{PC}$), the model has a current "saturation-based" ($\mathcal{PC} = \mathcal{PCS}$) and current "latching-based" ($\mathcal{PC} = \mathcal{PCL}$) protection. To have d-axis priority in the limiter, $\mathcal{PCS} = \mathcal{PCS}1$ for the "saturation-based" and $\mathcal{PCL} = \mathcal{PCL}1$ for the "latching-based" limiter can be selected. Similarly, to have q-axis priority in the limiter (as recommended in IEEE Std. 2800 [10]), $\mathcal{PCS} = \mathcal{PCS}2$ for the "saturation-based" and $\mathcal{PCL} = \mathcal{PCL}2$ for the "latching-based" limiter can be selected. The mathematical models of all these control logics are discussed in Section III.

III. Deep Dive Into the EMT Model of GFL IBRs

This section discusses the mathematical and computational models of the EMT model of GFL IBRs. In particular, the "controller logic" and "protection logic" are discussed in detail while referring to Table III, Table III, and Fig. 2.

A. Outer Power Controller [$\mathcal{CP}$]

As mentioned in the previous section, the outer power controller consists of the following controls: 1) open-loop PQ dispatch control, 2) closed-loop PQ dispatch control, and 3) DC-bus voltage ($V_{\rm dc}$) and AC terminal voltage ($V_{\rm ac}$) control.

1) Open-Loop PQ Dispatch Control [$\mathcal{CPP}1$ and $\mathcal{CPQ}1$]

An open-loop PQ dispatch controller generates the reference current signals for the inner current controller of the GFL IBR. The objective is to regulate the output active and reactive power of the GFL IBR to a pre-specified reference active power, $P_{\rm ref}$, and reactive power, $Q_{\rm ref}$, defined either locally or remotely. The power references, $P_{\rm ref}$, $Q_{\rm ref}$, and the output of the synchronous reference frame (SRF) phase-locked loop (PLL) [14], [15] with $v_{\rm C}^{\rm abc}$ as input are used to set the references for the current controllers [16]–[18]. The SRF PLL is based on aligning in closed-loop control the angle of the dq-transformation such that $v_{\rm C}^{\rm abc}$ has no q-axis component. A proportional-integral (PI) regulator acts on the alignment error to set the rotation frequency. The desired output current references are calculated using the following pair of equations:

- For $\mathcal{CPP}1$, $\mathcal{CPQ}1$ with $\mathcal{CC}1$:

$$i_{\rm L,ref}^{\rm d'} = \frac{v_{\rm C}^{\rm d}P_{\rm ref} + v_{\rm C}^{\rm q}Q_{\rm ref}}{(v_{\rm C}^{\rm d})^2 + (v_{\rm C}^{\rm q})^2},\ i_{\rm L,ref}^{\rm q'} = \frac{v_{\rm C}^{\rm q}P_{\rm ref} - v_{\rm C}^{\rm d}Q_{\rm ref}}{(v_{\rm C}^{\rm d})^2 + (v_{\rm C}^{\rm q})^2}. \quad (1)$$

- For $\mathcal{CPP}1$, $\mathcal{CPQ}1$ with $\mathcal{CC}2$:

$$i_{\rm L,ref}^{\alpha'} = \frac{v_{\rm C}^{\alpha}P_{\rm ref} + v_{\rm C}^{\beta}Q_{\rm ref}}{(v_{\rm C}^{\alpha})^2 + (v_{\rm C}^{\beta})^2},\ i_{\rm L,ref}^{\beta'} = \frac{v_{\rm C}^{\beta}P_{\rm ref} - v_{\rm C}^{\alpha}Q_{\rm ref}}{(v_{\rm C}^{\alpha})^2 + (v_{\rm C}^{\beta})^2}. \quad (2)$$

- For $\mathcal{CPP}1$, $\mathcal{CPQ}1$ with $\mathcal{CC}3$:

Using the SRF PLL output, $\theta_{\rm pll}$ and $-\theta_{\rm pll}$, the positive- and negative-sequence components of the voltage ($v_{\rm C}^{\rm d^+}$, $v_{\rm C}^{\rm d^-}$, $v_{\rm C}^{\rm q^+}$, $v_{\rm C}^{\rm q^-}$) and the current ($i_{\rm L}^{\rm d^+}$, $i_{\rm L}^{\rm d^-}$, $i_{\rm L}^{\rm q^+}$, $i_{\rm L}^{\rm q^-}$) are calculated using the method of [19]. For unbalanced voltage conditions, the following equation is used to create the commanded references for the current regulators:

$$\begin{bmatrix} i_{\rm L,ref}^{\rm d'^+} \\ i_{\rm L,ref}^{\rm q'^+} \\ i_{\rm L,ref}^{\rm d'^-} \\ i_{\rm L,ref}^{\rm q'^-} \end{bmatrix} = \begin{bmatrix} v_{\rm C}^{\rm d^+} & v_{\rm C}^{\rm q^+} & v_{\rm C}^{\rm d^-} & v_{\rm C}^{\rm q^-} \\ v_{\rm C}^{\rm q^+} & -v_{\rm C}^{\rm d^+} & v_{\rm C}^{\rm q^-} & -v_{\rm C}^{\rm d^-} \\ v_{\rm C}^{\rm d^-} & v_{\rm C}^{\rm q^-} & v_{\rm C}^{\rm d^+} & v_{\rm C}^{\rm q^+} \\ v_{\rm C}^{\rm q^-} & -v_{\rm C}^{\rm d^-} & -v_{\rm C}^{\rm q^+} & v_{\rm C}^{\rm d^+} \\ v_{\rm C}^{\rm q^-} & -v_{\rm C}^{\rm d^-} & v_{\rm C}^{\rm q^+} & -v_{\rm C}^{\rm d^+} \\ -v_{\rm C}^{\rm d^-} & -v_{\rm C}^{\rm q^-} & v_{\rm C}^{\rm d^+} & v_{\rm C}^{\rm q^+} \end{bmatrix}^{-1} \begin{bmatrix} P \\ Q \\ P_{\rm c} \\ P_{\rm s} \\ Q_{\rm c} \\ Q_{\rm s} \end{bmatrix} \quad (3)$$

where P and Q are the average real and reactive powers injected into the grid; and $P_{\rm c}$, $P_{\rm s}$, $Q_{\rm c}$, and $Q_{\rm s}$ are the magnitude of the double fundamental frequency oscillating real and reactive powers as quadrature components referenced to the synchronous rotating frame. The EMT model of GFL IBRs has flexibility in selecting the following types of sequence reference generation methods:

i) Active power ripple control: It generates $i_{\rm L,ref}^{\rm d'^+}$, $i_{\rm L,ref}^{\rm q'^+}$, $i_{\rm L,ref}^{\rm d'^-}$, and $i_{\rm L,ref}^{\rm q'^-}$ from (3) by setting $P_{\rm c} = P_{\rm s} = 0$.

ii) Reactive power ripple control: It generates $i_{\rm L,ref}^{\rm d'^+}$, $i_{\rm L,ref}^{\rm q'^+}$, $i_{\rm L,ref}^{\rm d'^-}$, and $i_{\rm L,ref}^{\rm q'^-}$ from (3) by setting $Q_{\rm c} = Q_{\rm s} = 0$.

iii) Balanced current control: It generates $i_{\rm L,ref}^{\rm d'^+}$, $i_{\rm L,ref}^{\rm q'^+}$, $i_{\rm L,ref}^{\rm d'^-}$, and $i_{\rm L,ref}^{\rm q'^-}$ from (3) by setting $P_{\rm c} = P_{\rm s} = Q_{\rm c} = Q_{\rm s} = 0$.

2) Closed-Loop PQ Dispatch Control [$\mathcal{CPP}2$ and $\mathcal{CPQ}2$]

Two PI controllers are used in the closed-loop PQ dispatch control. The set points are the commanded active power, $P_{\rm ref}$, and reactive power, $Q_{\rm ref}$ [13]; however, at the beginning, $v_{\rm C}^{\rm abc}$ and $i_{\rm O}^{\rm abc}$ are used to determine the instantaneous active power, p, and the instantaneous reactive power and then are passed through low-pass filters with the time constant, $\tau_{\rm S} \in \mathbb{R}_{>0}$, to obtain the average value of the active power, P, and the reactive power, Q. The desired output current references are calculated using the following pair of equations:

• For $\mathcal{CPP}2$, $\mathcal{CPQ}2$ with $\mathcal{CC}1$: The output of the PI regulators are directly used as $i^{\mathrm{d}'}_{\mathrm{L,ref}}$ and $i^{\mathrm{q}'}_{\mathrm{L,ref}}$.

• For $\mathcal{CPP}2$, $\mathcal{CPQ}2$ with $\mathcal{CC}2$: $i^{\mathrm{d}'}_{\mathrm{L,ref}}$ and $i^{\mathrm{q}'}_{\mathrm{L,ref}}$ are transformed into $i^{\alpha'}_{\mathrm{L,ref}}$ and $i^{\beta'}_{\mathrm{L,ref}}$ using θ_{pll}.

3) V_{dc}-V_{ac} Control [$\mathcal{CPP}3$ and $\mathcal{CPQ}3$]

The main control objective is to regulate the DC-bus voltage, V_{dc}, and the AC terminal voltage. The kernel of the voltage control is the real/reactive power controller by which P and Q can be independently controlled; therefore, to regulate the DC-bus voltage and AC terminal voltage, a feedback mechanism compares V_{dc} with its reference command, $V^{\mathrm{ref}}_{\mathrm{dc}}$, and V_{ac} with its reference command, $V^{\mathrm{ref}}_{\mathrm{ac}}$. Accordingly, it adjusts P_{ref} and Q_{ref} such that the net power exchanged with the DC-bus capacitor is kept at zero and the required reactive power support is provided to regulate the terminal AC voltage. In this application, when the DC source is the PV module, the $V^{\mathrm{ref}}_{\mathrm{dc}}$ is the output of the maximum power point tracking (MPPT) controller, V_{mppt}. Here, the perturb and observe method of MPPT is used [20].

B. Protection Logic

The following fault current limiter protection for the GFL IBR model is employed:

1) Saturation-Based Current Limiter [$\mathcal{PCS}$]

The instantaneous current saturation limiter [21] sets hard limits on the inductor current references, $i^{\mathrm{d}'}_{\mathrm{L,ref}}$ and $i^{\mathrm{q}'}_{\mathrm{L,ref}}$, for $\mathcal{CC}1$. Whereas, for $\mathcal{CC}2$, the hard limit is on $i^{\alpha'}_{\mathrm{L,ref}}$ and $i^{\beta'}_{\mathrm{L,ref}}$. The d-axis priority-based instantaneous current saturation limiter, $\mathcal{PCS}1$, for $\mathcal{CC}1$ follows the following equations [22]–[24]:

$$|i^{\mathrm{d}}_{\mathrm{L,ref}}| = \mathtt{min}(i_{\mathrm{sat}}, |i^{\mathrm{d}'}_{\mathrm{L,ref}}|),\ |i^{\mathrm{q}}_{\mathrm{L,ref}}| = \mathtt{min}(i'_{\mathrm{sat}}, |i^{\mathrm{q}'}_{\mathrm{L,ref}}|). \quad (4)$$

where, $i'_{\mathrm{sat}} = \sqrt{i^2_{\mathrm{sat}} - (i^{\mathrm{d}}_{\mathrm{L,ref}})^2}$ Similarly, the q-axis priority-based instantaneous current saturation limiter, $\mathcal{PCS}2$, for $\mathcal{CC}1$ is implemented too [25], [26]. An instantaneous hard current saturation limiter will clip the peak of the sinusoidal signal in case of $\mathcal{CC}2$. This will result in distortion output currents. A circular current saturation limiter is usually implemented for $\mathcal{CC}2$ with the following equations [27]–[29]:

$$i^{\alpha\beta}_{\mathrm{L,ref}} = \begin{cases} i^{\alpha'\beta'}_{\mathrm{L,ref}}, & \text{if } \sqrt{(i^{\alpha'}_{\mathrm{L,ref}})^2 + (i^{\beta'}_{\mathrm{L,ref}})^2} \le i_{\mathrm{sat}}, \\ i^{\alpha'\beta'}_{\mathrm{L,ref}} \dfrac{i_{\mathrm{sat}}}{\sqrt{(i^{\alpha'}_{\mathrm{L,ref}})^2 + (i^{\beta'}_{\mathrm{L,ref}})^2}}, & \text{otherwise.} \end{cases} \quad (5)$$

where i_{sat} is usually selected as 1.2–1.5 p.u. of the nominal current of the IBR.

2) Latching-Based Current Limiter [$\mathcal{PCL}$]

The latching current limiter allows a mode change in the current values in which the GFL IBR control switches to a predefined inductor fault current reference, i_{latch}, instead of the reference current signals [27], [28], [30]. It is held at that value until the inductor current reference magnitude drops below a reset threshold, i_{reset}. For $\mathcal{CC}1$, the limiter follows the following equations [31]:

$$i^{\mathrm{d}}_{\mathrm{L,ref}}, i^{\mathrm{q}}_{\mathrm{L,ref}} = \begin{cases} i^{\mathrm{d,sat}}_{\mathrm{L,ref}}, i^{\mathrm{q,sat}}_{\mathrm{L,ref}} & \text{if } i_{\mathrm{L,ref}} \ge i_{\mathrm{sat}}, \\ i^{\mathrm{d}'}_{\mathrm{L,ref}}, i^{\mathrm{q}'}_{\mathrm{L,ref}} & \text{if } i_{\mathrm{L,ref}} \le i_{\mathrm{latch}}, \end{cases} \quad (6)$$

where $i_{\mathrm{L,ref}}$=$\sqrt{(i^{\mathrm{d}'}_{\mathrm{L,ref}})^2 + (i^{\mathrm{q}'}_{\mathrm{L,ref}})^2}$. Also, the selection of $i^{\mathrm{d,sat}}_{\mathrm{L,ref}}$ and $i^{\mathrm{q,sat}}_{\mathrm{L,ref}}$ should satisfy $\sqrt{(i^{\mathrm{d,sat}}_{\mathrm{L,ref}})^2 + (i^{\mathrm{q,sat}}_{\mathrm{L,ref}})^2} = i_{\mathrm{sat}}$. In case of d-axis priority-based latching, $\mathcal{PCL}1$, for $\mathcal{CC}1$, $i^{\mathrm{d,sat}}_{\mathrm{L,ref}}$ and $i^{\mathrm{q,sat}}_{\mathrm{L,ref}}$ are selected as follows [32]:

$$i^{\mathrm{d,sat}}_{\mathrm{L,ref}} = \frac{i^{\mathrm{d}'}_{\mathrm{L,ref}}}{|i^{\mathrm{d}'}_{\mathrm{L,ref}}|} \times \mathtt{min}(|i^{\mathrm{d}'}_{\mathrm{L,ref}}|, i_{\mathrm{sat}}), \quad (7)$$

$$i^{\mathrm{q,sat}}_{\mathrm{L,ref}} = \frac{i^{\mathrm{q}'}_{\mathrm{L,ref}}}{|i^{\mathrm{q}'}_{\mathrm{L,ref}}|} \times \mathtt{min}(|i^{\mathrm{q}'}_{\mathrm{L,ref}}|, \sqrt{(i_{\mathrm{sat}})^2 - (i^{\mathrm{d,sat}}_{\mathrm{L,ref}})^2}. \quad (8)$$

Similarly, the q-axis priority-based latching, $\mathcal{PCL}2$, for $\mathcal{CC}1$, are implemented too [33]. The latching equation for $\mathcal{CC}2$ is selected as follows [31], [34]:

$$i^{\alpha\beta,\mathrm{lim}}_{\mathrm{L,ref}} = \begin{cases} i^{\alpha'\beta'}_{\mathrm{L,ref}} \dfrac{i_{\mathrm{sat}}}{i_{\mathrm{L,ref}}}, & \text{if } i_{\mathrm{L,ref}} \ge i_{\mathrm{sat}}, \\ i^{\alpha'\beta'}_{\mathrm{L,ref}}, & \text{if } i_{\mathrm{L,ref}} \le i_{\mathrm{latch}}, \end{cases} \quad (9)$$

where $i_{\mathrm{L,ref}}$=$\sqrt{(i^{\alpha'}_{\mathrm{L,ref}})^2 + (i^{\beta'}_{\mathrm{L,ref}})^2}$. To prevent the limit cycle behavior of the inserted nonlinearity, i_{latch} is selected to be less than i_{sat} yet greater than the current magnitude at rated power operation at the lowest nominal voltage [31].

C. Inner Current Controller Logic

As mentioned in the previous section, the inner current controller consists of inner current control in the dq domain ($\mathcal{CC}1$), $\alpha\beta$ domain ($\mathcal{CC}2$), sequence domain ($\mathcal{CC}3$).

1) Inner Current Control in the dq Domain [$\mathcal{CC}1$]

For GFL IBRs, the conventional inner current controller in the synchronous reference frame (i.e., dq-domain) architecture is employed [35]. For the inner current controller, $i^{\mathrm{d}}_{\mathrm{L,ref}}$ and $i^{\mathrm{q}}_{\mathrm{L,ref}}$ are provided as the reference signals to be tracked by the output signals $i^{\mathrm{d}}_{\mathrm{L}}$ and $i^{\mathrm{q}}_{\mathrm{L}}$, respectively. A PI compensator is used to track the reference of the dq-axis inductor current. For a desired time constant, τ_{c}, the parameters of the current controller are selected as $k^{\mathrm{p}}_{\mathrm{c}} = L_{\mathrm{f}}/\tau_{\mathrm{c}}$ and $k^{\mathrm{i}}_{\mathrm{c}} = R_{\mathrm{f}}/\tau_{\mathrm{c}}$. Depending on the switching frequency, τ_{c} is typically selected to range from 0.5–2 ms [13]. Additional feed-forward voltage signals, $v^{\mathrm{d}}_{\mathrm{C}}$ and $v^{\mathrm{q}}_{\mathrm{C}}$, and cross-coupling signals, $-\omega_{\mathrm{N}} L_{\mathrm{f}} i^{\mathrm{q}}_{\mathrm{L}}$ and $\omega_{\mathrm{N}} L_{\mathrm{f}} i^{\mathrm{d}}_{\mathrm{L}}$, facilitate the disturbance rejection capability. Here, ω_{N} is the nominal frequency in rad/s.

2) Inner Current control in the $\alpha\beta$ Domain [$\mathcal{CC}2$]

For GFL IBRs, the conventional inner current controller in the stationary reference frame (i.e., $\alpha\beta$-domain) architecture is employed [36]. For the inner current controller for GFL IBRs, $i^{\alpha}_{\mathrm{L,ref}}$ and $i^{\beta}_{\mathrm{L,ref}}$ are provided as the reference signals to be tracked by the signals i^{α}_{L} and i^{β}_{L}, respectively. Following the *internal-model principle*, the PR controller's only two gain parameters, $k^{\mathrm{p}}_{\mathrm{c}}$ and $k^{\mathrm{r}}_{\mathrm{c}}$, have been used. For a desired phase margin and to gain crossover frequency, the parameters of the voltage controller ($k^{\mathrm{p}}_{\mathrm{c}}$ and $k^{\mathrm{r}}_{\mathrm{c}}$) can be designed [13]. Similarly, feed-forward voltage signals, v^{α}_{C}, v^{β}_{C}, facilitate the disturbance rejection capability.

3) Inner Current Control in the Sequence Domain [$\mathcal{CC}3$]

For GFL IBRs, the sequence domain inner current controller in the synchronous reference frame (i.e., dq-domain) architecture is employed [37]. For the inner current controller, $i^{\mathrm{d}^+}_{\mathrm{L,ref}}$,

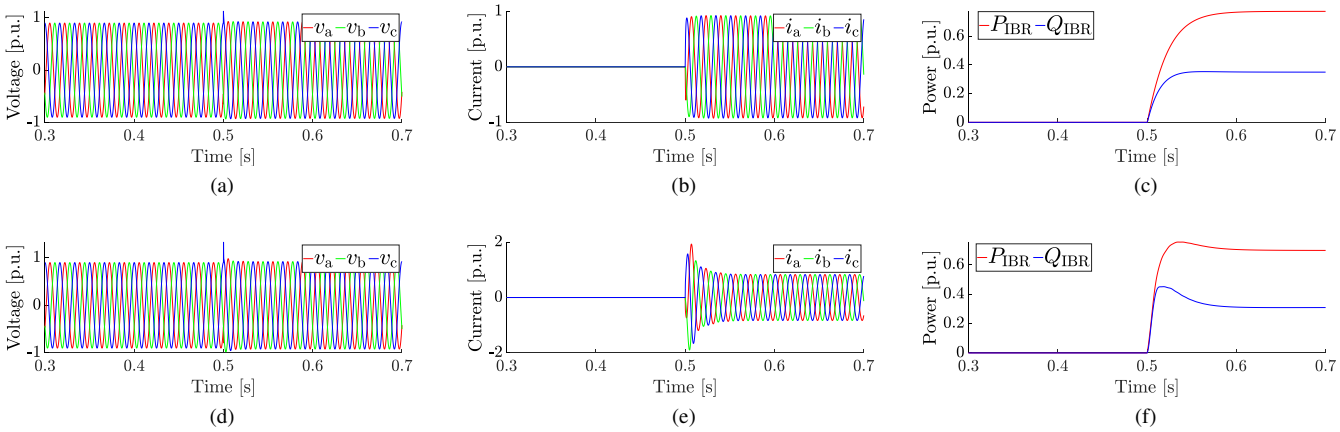

Fig. 3. Results of (a) AC terminal voltage, (b) inverter current, and (c) output active and reactive power of the GFL IBR model during $\mathcal{C}1$, and (d) AC terminal voltage, (e) inverter current, and (f) output active and reactive power of the GFL IBR model during $\mathcal{C}2$.

$i^{\mathrm{d}^-}_{\mathrm{L,ref}}$, $i^{\mathrm{q}^+}_{\mathrm{L,ref}}$, and $i^{\mathrm{q}^-}_{\mathrm{L,ref}}$ are provided as the reference signals to be tracked. The output signals are $i^{\mathrm{d}^+}_{\mathrm{L,ref}}$, $i^{\mathrm{d}^-}_{\mathrm{L,ref}}$, $i^{\mathrm{q}^+}_{\mathrm{L,ref}}$, and $i^{\mathrm{q}^-}_{\mathrm{L,ref}}$, and these are the notch filter outputs (resonant frequency at $2\omega_{\mathrm{pll}}$). The compensator and feed-forward signals are used here with the similar phenomenon of $\mathcal{CC}1$.

IV. Results

The generic GFL IBR model prototype is validated with comprehensive simulation testings in PSCAD. This section presents a few selected example simulation results. The simulations include the following four scenarios:

$\mathcal{C}1$) The averaged model inverter ($\mathcal{M}2$) is interfaced with the PV module ($\mathcal{S}1$) while running with closed-loop PQ dispatch control ($\mathcal{CPP}2$ and $\mathcal{CPQ}2$), with the inner current controller in the dq-domain ($\mathcal{CC}1$), and with the saturation-based current limiter $\mathcal{PCS}$ in the q-axis priority $\mathcal{PCS}2$. The GFL IBR was initially operating with P_{ref}=0 p.u. and Q_{ref}=0 p.u. At t=0.5 s, the P_{ref} jumps to 0.75 p.u. and Q_{ref} jumps to 0.33 p.u., in compliance with IEEE Std. 2800 [10].

$\mathcal{C}2$) The switching model inverter ($\mathcal{M}1$) is interfaced with the PV and battery module ($\mathcal{S}1$ and $\mathcal{S}2$) while running with closed-loop PQ dispatch control ($\mathcal{CPP}2$ and $\mathcal{CPQ}2$), with the sequence domain inner current controller ($\mathcal{CC}3$), and with latching current limiter $\mathcal{PCL}$ in the d-axis priority $\mathcal{PCL}1$. The GFL IBR was initially operating with P_{ref}=0 p.u. and Q_{ref}=0 p.u. At t=0.5 s, the P_{ref} jumps to 0.75 p.u. and Q_{ref} jumps to 0.33 p.u., in compliance with IEEE Std. 2800 [10].

$\mathcal{C}3$) The averaged model inverter ($\mathcal{M}2$) is interfaced with the PV module ($\mathcal{S}1$) while running with the closed-loop V_{dc}-Q and closed-loop control ($\mathcal{CPP}3$ and $\mathcal{CPQ}2$), with the inner current controller in the dq-domain ($\mathcal{CC}1$), and with the latching-based current limiter $\mathcal{PCL}$ in the q-axis priority $\mathcal{PCL}2$. The GFL IBR was initially operating with P_{ref}=0.75 p.u. and Q_{ref}=0.33 p.u. At t=0.5 s, a three-phase-to-ground (abcg) fault occurs with a fault resistance of 0.01Ω.

$\mathcal{C}4$) The switching model inverter ($\mathcal{M}1$) is interfaced with the PV module and battery module ($\mathcal{S}1$ and $\mathcal{S}2$) while running with the closed-loop V_{dc}-Q and closed-loop control ($\mathcal{CPP}3$ and $\mathcal{CPQ}2$), with the inner current controller in the sequence domain ($\mathcal{CC}3$), and with saturation-based current limiter $\mathcal{PCS}$ in the q-axis priority $\mathcal{PCS}2$. The GFL IBR was initially operating with P_{ref}=0.75 p.u. and Q_{ref}=0.33 p.u. At t=0.5 s, ABCG fault occurs with a fault resistance of 0.01Ω.

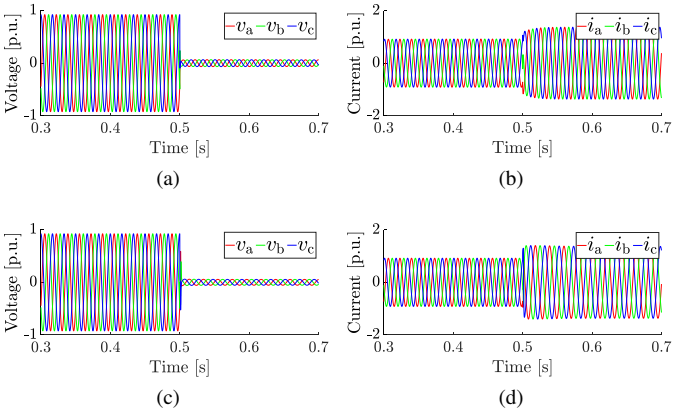

Fig. 4. Results of (a) output active power and (b) output reactive power of the GFL IBR model during $\mathcal{C}3$, and (c) output active power and (d) output reactive power of the GFL IBR model during $\mathcal{C}4$.

Fig. 3(a), Fig. 3(b), and Fig. 3(c) illustrate the results of the AC terminal voltage, inverter output current, and output active and reactive power of the GFL IBR model during $\mathcal{C}1$. Similarly, Fig. 3(d), Fig. 3(e), and Fig. 3(f) illustrate the results of the AC terminal voltage, inverter output current, and output active and reactive power of the GFL IBR model during $\mathcal{C}2$. In both the cases, the GFL IBR is able to inject the required amount of active and reactive power into the grid. Note that the inner current controller in the case of $\mathcal{C}1$ is different from $\mathcal{C}2$, and that drives the transient current behavior during the power reference jump, as observed in Fig. 3(b) and Fig. 3(e).

Fig. 4(a) and Fig. 4(b) illustrate the results of the output active power and output reactive power of the GFL IBR model during $\mathcal{C}3$. Similarly, Fig. 4(c) and Fig. 4(d) illustrate the results of the output active power and output reactive power of the GFL IBR model during $\mathcal{C}4$. In both the cases, due to the low impedance fault, the terminal voltage across the GFL IBR significantly drops, as expected; however, due to

respective current limiters ($\mathcal{PCL}2$ for $\mathcal{C}3$ and $\mathcal{PCS}2$ for $\mathcal{C}4$), the fault current contribution of the GFL IBR is not high and is restricted to the selected $i_{\rm sat}$ value (in this case, 1.2 p.u.). Therefore, in conclusion, the developed model of the GFL IBR successfully restricts the fault current to the safe upper limit.

V. CONCLUSION

This article presents a generic, easy-to-scale-up MVA rating, multifunctional, EMT dynamic model of GFL IBRs using the PSCAD software platform that complies with IEEE Std. 2800. The developed model includes features such as flexibility in selecting various types and combinations of DC sources, flexibility in selecting either the switching or averaged model of the inverter, and exhaustive lists of controller and protection logic. The generality in the power circuits and the multifunctional options in the operation and control of the developed EMT model make it suitable for both academia and industry to study various power system aspects. The developed model provides the user the option to study the impact of IBR power circuits and control and protection schemes on the fault behavior and will be of use to protection engineers to design protection systems. Moreover, for transient stability analysis and for steady-state and transient operation and control of power systems interfaced with various types of GFL IBRs, this model can be used with ease and flexibility in selecting various control and protection schemes as well as types of inverter models and DC sources. A few simulation case studies are also provided to showcase the performance of the model.

REFERENCES

[1] Y. Gu and C. T. Green, "Power system stability with a high penetration of inverter-based resources," in *Proceedings of the IEEE*, vol. 111, no. 7, 2023, pp. 832–853.

[2] L. Fan and Z. Miao, "Modeling and stability analysis of inverter-based resources," *CRC Press*, pp. 1–286, 2023.

[3] A. Zamzam and J. Wang, "Hierarchical data-driven protection for microgrid with 100% renewable penetration," in *IEEE Energy Conversion Congress and Exposition (ECCE)*, 2023, pp. 1–8.

[4] N. Hatziargyriou *et al.*, "Definition and classification of power system stability – revisited & extended," *IEEE Tran. Power Systems*, vol. 36, no. 4, pp. 3271–3281, 2021.

[5] Y. N. Velaga *et al.*, "Transient stability study of a real-world microgrid with 100% renewables," in *IEEE Energy Conversion Congress and Exposition (ECCE)*, 2022, pp. 1–8.

[6] "IEEE standard for interconnection and interoperability of distributed energy resources with associated electric power systems interfaces," *IEEE Std 1547-2018 (Revision)*, pp. 1–138, 2018.

[7] R. W. Kenyon, A. Sajadi, A. Hoke, and B.-M. Hodge, "Open-source pscad grid-following and grid-forming inverters and a benchmark for zero-inertia power system simulations," in *2021 IEEE Kansas Power and Energy Conference (KPEC)*, 2021, pp. 1–6.

[8] S. Debnath, J. Choi, H. Hughes, K. Kurte, P. Marthi, and S. Hahn, "High-performance computing based emt simulation of large pv or hybrid pv plants," in *2023 IEEE Power & Energy Society General Meeting (PESGM)*, 2023, pp. 1–5.

[9] "Generic photovoltaic inverter model in an electromagnetic transients simulator for transmission connected plants," pp. 1–100, 2022.

[10] "IEEE standard for interconnection and interoperability of inverter-based resources (ibrs) interconnecting with associated transmission electric power systems," *IEEE Std 2800-2022*, pp. 1–180, 2022.

[11] R. Teodorescu, Liserre, and P. Marco, Rodriguez, "Grid converters for photovoltaic and wind power systems," *IEEE Wiley*, pp. 1–407, 2011.

[12] P. T. Krein, J. Bentsman, R. M. Bass, and B. L. Lesieutre, "On the use of averaging for the analysis of power electronic systems," *IEEE Transactions on power electronics*, vol. 5, no. 2, pp. 182–190, 1990.

[13] A. Yazdani and R. Iravani, *Voltage-sourced converters in power systems: modeling, control, and applications*. John Wiley & Sons, 2010.

[14] S. Golestan, J. M. Guerrero, and J. C. Vasquez, "Three-phase plls: A review of recent advances," *IEEE Transactions on Power Electronics*, vol. 32, no. 3, pp. 1894–1907, 2016.

[15] S. Ke and Y. Li, "Grid-connected phase-locked loop technology based on a cascade second-order iir filter," *Energies*, vol. 16, p. 3967, 2023.

[16] e. a. Blaabjerg, Frede, "Overview of control and grid synchronization for distributed power generation systems," *IEEE Transactions on industrial electronics*, vol. 53, no. 5, pp. 1398–1409, 2006.

[17] A. Khan, M. Easley, M. Hosseinzadehtaher, M. B. Shadmand, H. Abu-Rub, and P. Fajri, "Pll-less active and reactive power controller for grid-following inverter," in *2020 IEEE Energy Conversion Congress and Exposition (ECCE)*. IEEE, 2020, pp. 4322–4328.

[18] N. Kroutikova, C. A. Hernandez-Aramburo, and T. C. Green, "State-space model of grid-connected inverters under current control mode," *IET Electric Power Applications*, vol. 1, no. 3, pp. 329–338, 2007.

[19] R. Kabiri, D. G. Holmes, and B. P. McGrath, "Control of active and reactive power ripple to mitigate unbalanced grid voltages," *IEEE Transactions on Industry Applications*, vol. 52, pp. 1660–1668, 2015.

[20] e. a. Elgendy, Mohammed A., "Assessment of perturb and observe mppt algorithm implementation techniques for pv pumping applications," *IEEE Transactions on Sustainable Energy*, vol. 3, pp. 21–33, 2012.

[21] N. Bottrell and T. C. Green, "Comparison of current-limiting strategies during fault ride-through of inverters to prevent latch-up and wind-up," *IEEE Transactions on Power Electronics*, vol. 29, pp. 3786–3797, 2013.

[22] T. Qoria, F. Gruson, F. Colas, X. Kestelyn, and X. Guillaud, "Current limiting algorithms and transient stability analysis of grid-forming vscs," *Electric Power Systems Research*, vol. 189, p. 106726, 2020.

[23] L. Huang, H. Xin, Z. Wang, L. Zhang, K. Wu, and J. Hu, "Transient stability analysis and control design of droop-controlled voltage source converters considering current limitation," *IEEE Transactions on Smart Grid*, vol. 10, no. 1, pp. 578–591, 2017.

[24] S. Li, L. Xu, and T. A. Haskew, "Control of vsc-based statcom using conventional and direct-current vector control strategies," *International Journal of Electrical Power & Energy Systems*, pp. 175–186, 2013.

[25] X. Zhao and D. Flynn, "Freezing grid-forming converter virtual angular speed to enhance transient stability under current reference limiting," in *2020 IEEE 21st Workshop on Control and Modeling for Power Electronics (COMPEL)*. IEEE, 2020, pp. 1–7.

[26] ——, "Stability enhancement strategies for a 100% grid-forming and grid-following converter-based irish power system," *IET Renewable Power Generation*, vol. 16, no. 1, pp. 125–138, 2022.

[27] M. G. Taul, X. Wang, P. Davari, and F. Blaabjerg, "Current limiting control with enhanced dynamics of grid-forming converters during fault conditions," *IEEE Journal of Emerging and Selected Topics in Power Electronics*, vol. 8, no. 2, pp. 1062–1073, 2019.

[28] C. Liu, X. Cai, R. Li, and R. Yang, "Optimal short-circuit current control of the grid-forming converter during grid fault condition," *IET Renewable Power Generation*, vol. 15, no. 10, pp. 2185–2194, 2021.

[29] M. Awal and I. Husain, "Transient stability assessment for current-constrained and current-unconstrained fault ride through in virtual oscillator-controlled converters," *IEEE Journal of Emerging and Selected Topics in Power Electronics*, vol. 9, no. 6, pp. 6935–6946, 2021.

[30] C. A. Plet and T. C. Green, "A method of voltage limiting and distortion avoidance for islanded inverter-fed networks under fault," in *European Conference on Power Electronics and Applications*, 2011, pp. 1–8.

[31] ——, "Fault response of inverter interfaced distributed generators in grid-connected applications," *EPSR*, vol. 106, pp. 21–28, 2014.

[32] K. G. Saffar, S. Driss, and F. B. Ajaei, "Impacts of current limiting on the transient stability of the virtual synchronous generator," *IEEE Transactions on Power Electronics*, vol. 38, no. 2, pp. 1509–1521, 2022.

[33] B. Fan and X. Wang, "Fault recovery analysis of grid-forming inverters with priority-based current limiters," *IEEE Transactions on Power Systems*, 2022.

[34] B. Fan, T. Liu, F. Zhao, H. Wu, and X. Wang, "A review of current-limiting control of grid-forming inverters under symmetrical disturbances," *IEEE Open Journal of Power Electronics*, 2022.

[35] B. Bahrani, S. Kenzelmann, and A. Rufer, "Multivariable-pi-based *dq* current control of voltage source converters with superior axis decoupling capability," *IEEE Transactions on Industrial Electronics*, vol. 58, no. 7, pp. 3016–3026, 2010.

[36] D. N. Zmood and D. G. Holmes, "Stationary frame current regulation of pwm inverters with zero steady-state error," *IEEE Transactions on power electronics*, vol. 18, no. 3, pp. 814–822, 2003.

[37] B. Mahamedi, M. Eskandari, J. E. Fletcher, and J. Zhu, "Sequence-based control strategy with current limiting for the fault ride-through of inverter-interfaced distributed generators," *IEEE Transactions on Sustainable Energy*, vol. 11, no. 1, pp. 165–174, 2018.